

# Neutral scalar pair productions through $W$ -boson fusion at multi-TeV muon colliders

Khiem Hong Phan<sup>a,b</sup>, Quang Hoang-Minh Pham<sup>c</sup>

<sup>a</sup>*Institute of Fundamental and Applied Sciences, Duy Tan University, Ho Chi Minh City 70000, Vietnam*

<sup>b</sup>*Faculty of Natural Sciences, Duy Tan University, Da Nang City 50000, Vietnam*

<sup>c</sup>*VNUHCM-University of Science, 227 Nguyen Van Cu, District 5, Ho Chi Minh City 70000, Vietnam*

---

## Abstract

Full one-loop electroweak radiative corrections to  $\mu^-\mu^+ \rightarrow W^\pm W^\mp \rightarrow hh$  in the Standard Model are computed for the first time in this work. We then evaluate neutral scalar pair production through vector boson fusion at multi-TeV muon colliders within Two-Higgs-Doublet Model (THDM). In the phenomenological analysis, the enhancement factor, defined as the ratio of the cross sections for SM-like Higgs pair production in the THDM with respect to the corresponding ones in the SM, is examined over the viable regions of the parameter space in the Type-X and Type-Y THDMs. Our findings show that this ratio can reach a factor of 3 in several regions within the valid parameter space of the Type-X THDM, whereas it ranges from 0.91 to 0.96 over the entire parameter space of the Type-Y THDM. Finally, we scan the cross sections for double CP-odd Higgs production over the updated parameter space of the Type-X and Type-Y THDMs. In the Type-Y case at  $\sqrt{s} = 10$  TeV with an integrated luminosity of  $\mathcal{L} = 10000 \text{ fb}^{-1}$ , CP-odd Higgs pair production in the  $t\bar{t}b\bar{b}$  final state, with subsequent top-quark decays into leptons and bottom quarks taken into account, can be tested with a statistical significance exceeding the  $2\sigma$  level at several viable parameter points.

*Keywords:* Higgs boson phenomenology, physics beyond the Standard Model, and new physics at present and future multi-TeV muon colliders.

---

## 1. Introduction

Measurements of multi-scalar Higgs production are among the main objectives at future colliders, including the High-Luminosity Large Hadron Collider (HL-LHC), future  $e^+e^-$  lepton colliders, and future multi-TeV muon colliders. The measured data allows us to verify the structure of the scalar Higgs potential and offers deeper insight into the electroweak symmetry-breaking mechanism (EWSB) in particle physics. The ATLAS Collaboration has searched for SM-like Higgs boson pair production in the  $b\bar{b}\gamma\gamma$  events at  $\sqrt{s} = 13$  TeV in  $pp$  collisions at the LHC [1, 2]. Additional measurements for SM-like Higgs boson pair production in association with a vector boson ( $W$  or  $Z$ ) at  $\sqrt{s} = 13$  TeV have also been performed by the LHC [3]. The CMS Collaboration has investigated nonresonant Higgs boson pair production in the four-bottom-quark final state in  $pp$  collisions, as reported in Refs. [4, 5]. Further measurements of nonresonant Higgs boson pair production in the  $b\bar{b}\tau^-\tau^+$  [6] and four-bottom-quark [7] final states have been conducted by the ATLAS Collaboration. A combined analysis of the  $b\bar{b}\gamma\gamma$ ,  $b\bar{b}\tau^-\tau^+$ , and  $b\bar{b}b\bar{b}$  channels has been presented in Ref. [8]. The studies of Higgs pair production through different final states have been also carried out in Refs. [9, 10, 11, 12, 13, 14, 15].

---

*Email address:* phanhongkhiem@duytan.edu.vn (Khiem Hong Phan)

Phenomenological studies of Higgs boson pair production at the colliders within the SM and its extensions have been performed. In particular, di-Higgs production in the THDM has been investigated at the LHC in parameter regions consistent with the diphoton excess and the muon ( $g - 2$ ) anomaly [16]. Theoretical implications for Higgs boson pair production in the  $b\bar{b}\mu^+\mu^-$  final state at the LHC have been discussed in Ref. [17]. Moreover, probing the electroweak sector using the process  $W_L W_L \rightarrow n \times h$  has been examined within various effective field theory (EFT) frameworks [18]. Theoretical predictions for di-Higgs production in final states with two  $b$ -tagged jets, two leptons, and missing transverse momentum at the HL-LHC have also been carried out in Ref. [19]. Furthermore, double Higgs production via  $W$ -boson fusion at TeV-scale  $e^+e^-$  colliders has been investigated within effective field theory (EFT) frameworks, including studies of sensitivity to BSM Higgs couplings [20], multi-Higgs measurements in the SMEFT [21], additional analyses of Higgs boson pair production in EFTs [22], as well as in extended Higgs sector models [23]. Di-Higgs production has been studied in the Higgs singlet extension [24] and the I(1+2)HDM Type-I [25]. Further investigations in various BSM frameworks include vector-boson-fusion di-Higgs production in the SMEFT [26], enhancements from TeV-scale heavy neutral leptons at future lepton colliders [27], and scenarios involving axion-like particles [28]. The potential of probing new physics through di-Higgs production at the LHC has also been explored in Ref. [29].

Higher-order corrections to Higgs boson pair production are also of great interest in the literature. In particular, QCD corrections to Higgs boson pair production, including decays into the  $b\bar{b}\tau^+\tau^-$  final state, have been reported in Ref. [30]. In addition, double-logarithmic enhancements in Higgs boson pair production in the high-energy limit have been studied in Ref. [31]. Next-to-leading-order electroweak corrections have been presented in Refs. [32, 33], while higher-order corrections to Higgs boson pair production within the Higgs Effective Field Theory (HEFT) framework have been studied in Refs. [34, 35], as well as top-Yukawa- and light-quark-induced electroweak corrections in Ref. [36]. Furthermore, NLO QCD and electroweak corrections to double Higgs production have been computed in Refs. [37, 38, 39, 40, 41, 42, 43, 44, 45, 46, 47, 48, 50].

It is clear that future lepton colliders (LCs) could provide a cleaner environment than hadron colliders, which are affected by large QCD backgrounds. For this reason, future LCs allow for higher-precision measurements. Another aspect is that future multi-TeV muon colliders are proposed to access a higher-energy regime, enabling probes of new physics. Since scalar particles couple directly to vector bosons, vector boson fusion processes at multi-TeV muon colliders provide an excellent probe of additional scalar states predicted in many BSM scenarios, potentially enhancing the cross sections through  $s$ -channel resonance effects. For the above reasons, multi-TeV muon colliders could offer excellent prospects for measurements of double scalar production processes. So far, no calculations including full one-loop electroweak corrections for double scalar production via  $W$ -boson fusion have been reported. In this work, we evaluate for the first time full one-loop electroweak radiative corrections to the process  $\mu^-\mu^+ \rightarrow W^\pm W^\mp \rightarrow hh$  in the Standard Model. Neutral scalar pair productions through vector  $W$ -boson fusion at multi-TeV muon colliders within Two-Higgs-Doublet Models (THDM) are then computed and the corresponding cross sections are scanned over the updated parameter space of type-X and type-Y THDMs. The enhancement factor defined as the ratio of the cross sections for SM-like Higgs pair productions in the THDM with respect to the corresponding ones in the SM is examined over the viable region of parameters in the types of the THDM. Finally, CP-odd Higgs pair production is studied over the parameter space of the models under investigation. In the Type-Y case at  $\sqrt{s} = 10$  TeV with an integrated luminosity of  $\mathcal{L} = 10000 \text{ fb}^{-1}$ , CP-odd Higgs pair production in the  $t\bar{t}b\bar{b}$  final state, with subsequent top-quark decays into leptons and bottom

quarks taken into account, can be tested with a statistical significance exceeding the  $2\sigma$  level at several viable parameter points.

The outline of this paper is as follows. In Section 2, we present the THDM and discuss the relevant constraints. Full one-loop electroweak radiative corrections to the process  $\mu^- \mu^+ \rightarrow W^\pm W^\mp \rightarrow hh$  in the SM are computed in detail in Section 3. Phenomenological studies are presented in Section 4. Finally, the conclusions and outlooks are given in Section 5. Checks of the calculations are reported in the appendices.

## 2. The Two-Higgs-Doublet Model and Its Constraints

The structure of the models under investigation and the corresponding constraints are presented in this section. For further reviews of the THDM, including phenomenological studies, we refer the reader to Refs. [51, 52, 53, 54, 55]. In particular, the gauge and fermion contents of the THDM remain the same as in the SM. In contrast, the scalar Higgs sector is modified by introducing an additional scalar field with hypercharge  $Y = 1/2$ . With the addition of this scalar Higgs field, the most general scalar Higgs potential consistent with gauge invariance and renormalizability, and preserving a discrete  $Z_2$  symmetry, reads as follows (adopting the same notation as in Ref. [53]):

$$\begin{aligned} \mathcal{V}(\Phi_1, \Phi_2) = & \sum_{j=1}^2 m_{jj}^2 \Phi_j^\dagger \Phi_j - \left( m_{12}^2 \Phi_1^\dagger \Phi_2 + \text{H.c.} \right) + \frac{1}{2} \sum_{j=1}^2 \lambda_j \left( \Phi_j^\dagger \Phi_j \right)^2 \\ & + \lambda_3 \Phi_1^\dagger \Phi_1 \Phi_2^\dagger \Phi_2 + \lambda_4 \Phi_1^\dagger \Phi_2 \Phi_2^\dagger \Phi_1 + \left[ \frac{1}{2} \lambda_5 \left( \Phi_1^\dagger \Phi_2 \right)^2 + \text{H.c.} \right]. \end{aligned} \quad (1)$$

As in our earlier works [51, 52, 53, 54], the CP-conserving version of the THDM is employed for the phenomenological analysis. Consequently, all parameters,  $m_{11}^2$ ,  $m_{22}^2$ ,  $m_{12}^2$ , and  $\lambda_1, \dots, \lambda_5$ , are taken to be real. In addition, a discrete  $Z_2$  symmetry is introduced in the scalar potential, with only the allowed soft-breaking term, to explain the absence of tree-level flavor-changing neutral currents. As a result, four distinct types of THDMs are classified according to their different Yukawa coupling structures. Following Ref. [51], the general form of the Yukawa Lagrangian is taken as follows:

$$\begin{aligned} -\mathcal{L}_Y = & \sum_{f=u,d,\ell} \left( \sum_{\phi_j=h,H} \frac{m_f}{v} \xi_{\phi_j}^f \phi_j \bar{f} f - i \frac{m_f}{v} \xi_A^f \bar{f} \gamma_5 f A \right) \\ & + \frac{\sqrt{2}}{v} [\bar{u}_i V_{ij} (m_{u_i} \xi_A^u P_L + \xi_A^d m_{d_j} P_R) d_j H^+] \\ & + \frac{\sqrt{2}}{v} \bar{\nu}_L \xi_A^\ell m_{\ell} \ell_R H^+ + \text{H.c.} \end{aligned} \quad (2)$$

Where  $v$  denotes the vacuum expectation value. The Cabibbo–Kobayashi–Maskawa (CKM) matrix, with elements  $V_{ij}$ , is taken into account in the above Lagrangian to describe quark mixing. The operators  $P_{L/R} = \frac{1 \mp \gamma_5}{2}$  correspond to projection operators, and the left- and right-handed leptons are denoted by  $\ell_{L/R}$ . The coupling coefficients appearing in Eq. 2 are listed in Table 2 of Ref. [56].

After the EWSB, additional scalar particles in the considered model include a CP-even Higgs ( $H$ ), a CP-odd Higgs ( $A$ ), and two singly charged Higgs bosons ( $H^\pm$ ). It is noted that the independent parameters in the THDM used in our analysis consist of the mixing angles  $s_{\beta-\alpha}$

and  $t_\beta$ , the scalar masses  $m_H$ ,  $m_A$ , and  $m_{H^\pm}$ , as well as the soft-breaking parameter  $m_{12}^2$ . Before proceeding to the study of neutral scalar pair production at multi-TeV muon colliders, we first provide an overview of the updated parameter space of the considered model. The six independent parameters of the THDM are constrained by both theoretical and experimental bounds. For a detailed discussion of these constraints and the corresponding results, we refer the reader to our previous works, Refs. [51, 52, 53]. The parameters are scanned over the following ranges:  $m_h = 125.09$  GeV,  $m_H \in [130, 1000]$  GeV,  $s_{\beta-\alpha} \in [0.97, 1]$ ,  $m_{A,H^\pm} \in [130, 1000]$  GeV,  $t_\beta \in [0.5, 45]$ , and  $m_{12}^2 \in [0, 10^6]$  GeV<sup>2</sup>. The theoretical conditions are first imposed to scan the above parameter ranges with including perturbative unitarity, perturbativity, and vacuum stability of the model under investigation. The valid data points are then tested against electroweak precision observables (EWPOs). In this test, the electroweak oblique parameters  $S$ ,  $T$ , and  $U$  [57], which are related to the  $W$ -boson mass [66], are taken into account. The allowed parameter space is obtained by requiring the  $S$ ,  $T$ , and  $U$  parameters to bound within the 95% confidence level limits. It is worth mentioning that we employ 2HDMC-1.8.0 [58] for all the aforementioned analyses. Furthermore, to check that the theoretical predictions of the model under study are consistent with exclusion limits from Higgs searches at LEP, the LHC, and the Tevatron, we employ the public code `HiggsBounds-5.10.1` [59]. This program matches theoretical predictions to experimental upper limits from collider searches established at the 95% confidence level. Additionally, it is required that the theoretical predictions for the SM-like Higgs boson in the model be compatible with the corresponding experimental measurements at the LHC. To validate these constraints, we use the public code `HiggsSignals-2.6.1` [60]. Finally, experimental constraints from flavor physics are taken into account, in particular those arising from  $B$ -meson observables measured by LHCb. These constraints are using the `SuperISO v4.1` package [61], and only parameter points whose theoretical predictions are compatible with the corresponding experimental data within the  $2\sigma$  bounds retained.

Using the updated parameter-space data files provided in Refs. [51, 52, 53], we present several representative scatter plots that are used in the subsequent analysis. In Fig. 1, the parameter space of the six independent parameters is shown for the Type-X THDM (left) and the Type-Y THDM (right). The upper panels display scatter plots of  $m_A - m_H$ ,  $m_{H^\pm} - m_H$ , and  $m_{H^\pm} - m_A$ , while the lower panels show scatter plots of  $m_{12}^2$ ,  $m_A$  and the mixing angle  $\tan\beta$ . The results shown in the upper panels indicate that the mass splittings among any two of the three scalar states are required to be smaller than approximately  $\sim 200$  GeV due to the EWPO constraints. In the Type-X scenario, the mass splitting between the charged Higgs boson and the CP-even Higgs boson can reach values as large as  $\pm 600$  GeV. Nevertheless, the dominant region in the  $m_{H^\pm} - m_A$  plane is concentrated in the green-shaded area, indicating that  $m_{H^\pm} \simeq m_A$  in this case. Similar features are observed for the mass splittings in the Type-Y THDM. In this case, the allowed range of the mass difference is  $-600 \text{ GeV} \leq m_A - m_H \leq 400 \text{ GeV}$ , which is narrower than the corresponding range  $-600 \text{ GeV} \leq m_A - m_H \leq 600 \text{ GeV}$  found in the Type-X scenario. In the lower panels, we present scatter plots of  $m_{12}^2$ ,  $m_A$ , and  $\tan\beta$  for the Type-X THDM (left) and the Type-Y THDM (right). Over the full range of CP-odd Higgs masses, the soft  $Z_2$ -breaking parameter  $m_{12}^2$  lies in the range  $3 \cdot 10^3 \leq m_{12}^2 \leq 5 \cdot 10^5$  for both THDM types. From these plots, we also find that  $1 \leq \tan\beta \leq 20$ .

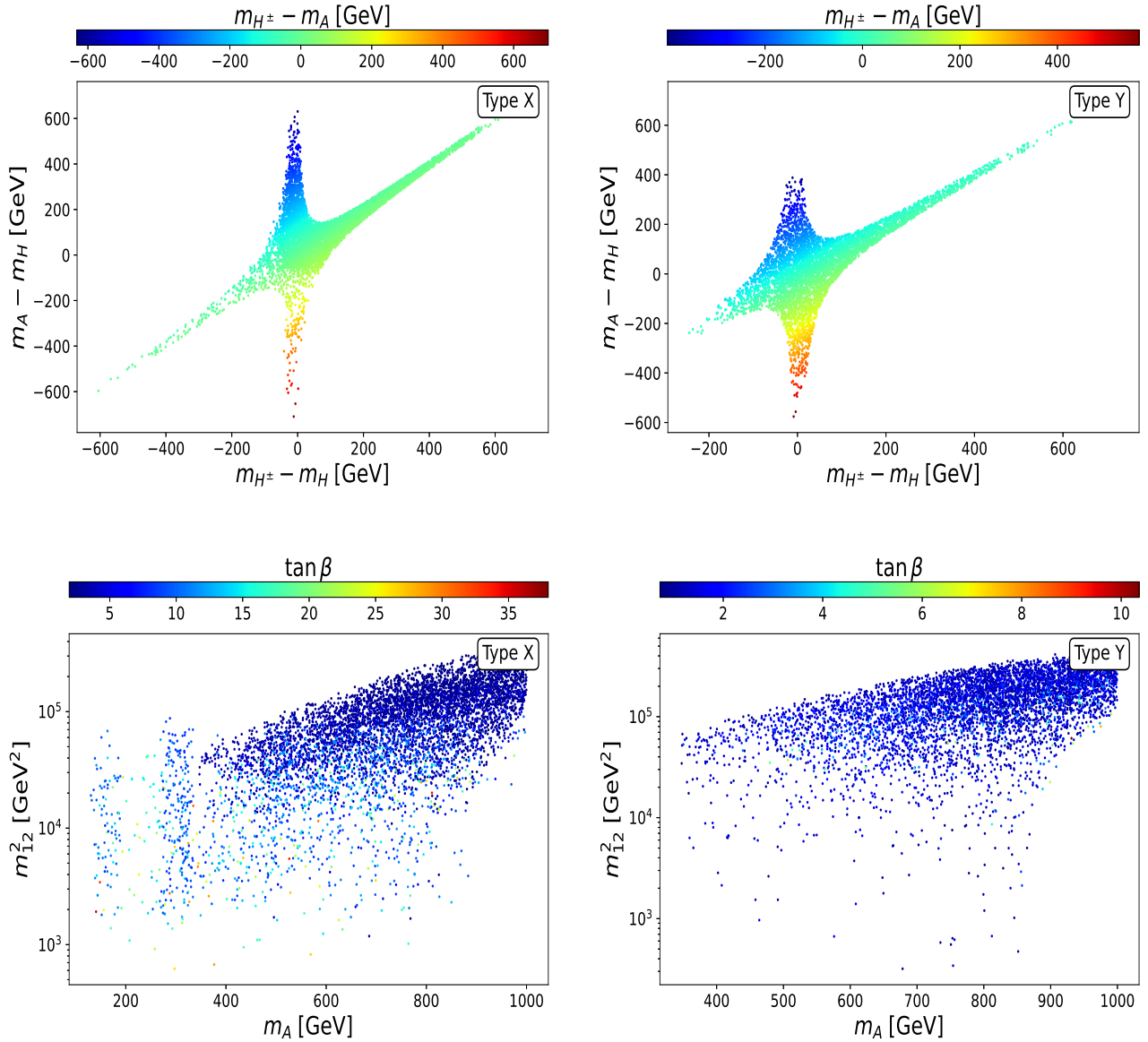


Figure 1: The parameter space for six independent parameters of THDM type-X on the left and type-Y on the right. The upper-plots show for scatter plots of  $m_A - m_H, m_{H^\pm} - m_H$  and  $m_{H^\pm} - m_A$ . While lower-plots are for scatter plots of  $m_{12}^2, m_A$  and the mixing angle  $t_B$ .

### 3. One-loop radiative corrections to $\mu^- \mu^+ \rightarrow W^\pm W^\mp \rightarrow hh$ in SM

In this section, we present the first calculations for full one-loop radiative corrections to  $\mu^- \mu^+ \rightarrow W^\pm W^\mp \rightarrow hh$  within the SM in this work. The calculations are performed with the help of the GRACE-Loop system, which is described in detail in Ref. [62]. In general, the total cross section for the process  $\mu^- \mu^+ \rightarrow VV \rightarrow hh$  can be computed as follows:

$$\sigma_{\mu^- \mu^+ \rightarrow VV \rightarrow hh}(s) = \sum_{\lambda_1, \lambda_2} \int_{4m_h^2/s}^1 d\tau \int_{\tau}^1 \frac{d\xi}{\xi} f_{V_{\lambda_1}/\mu}(\xi, Q^2) f_{V_{\lambda_2}/\mu}\left(\frac{\tau}{\xi}, Q^2\right) \hat{\sigma}_{V_{\lambda_1} V_{\lambda_2} \rightarrow hh}(\hat{s} = \tau s). \quad (3)$$

Where  $\hat{\sigma}_{V_{\lambda_1} V_{\lambda_2} \rightarrow hh}(\tau s)$  is the corresponding cross section for the partonic process  $V_{\lambda_1} V_{\lambda_2} \rightarrow hh$ .  $\lambda_1$  and  $\lambda_2$  are the polarization degrees of the vector bosons. In this work, the partonic processes are evaluated including one-loop radiative corrections using the **GRACE-Loop** system. Moreover, the vector-boson  $V$  splitting functions describe the probability for the emission of a weak vector boson from muon which is so-called as the helicity-dependent parton distribution functions (PDFs) are given by

$$f_{V/\mu}(\xi, Q^2) = \frac{g_V^2}{16\pi^2} \left[ \frac{1 + (1-x)^2}{x} \ln \left( \frac{Q^2}{m_V^2} \right) + \frac{2(1-x)}{x} \right]. \quad (4)$$

Where  $Q^2$  is energy scale. We emphasize that the first term corresponds to the transverse polarization of vector boson PDF, while the second term corresponds to the longitudinal polarization of the vector boson PDF. The coupling coefficient  $g_V$  is taken as  $g_V^2 = \frac{g^2}{2}$  for  $V = W^\pm$ , and  $g_V^2 = \frac{g^2}{c_W^2} \left[ (-1/2 + s_W^2)^2 + s_W^4/2 \right]$  for  $V = Z$ . In general, several types of partonic subprocesses are considered in this work, namely  $\gamma\gamma \rightarrow hh$ ,  $\gamma Z \rightarrow hh$ ,  $ZZ \rightarrow hh$ , and  $W^\pm W^\pm \rightarrow hh$ . However, the first two channels are loop-induced processes and are therefore expected to give smaller contributions compared to the latter processes. It is well known that the  $ZZ$ -fusion process proceeds as  $\mu^- \mu^+ \rightarrow ZZ \rightarrow \mu^- \mu^+ hh$ , while the  $WW$ -fusion channel is given by  $\mu^- \mu^+ \rightarrow W^\pm W^\mp \rightarrow \nu_\mu \bar{\nu}_\mu hh$ . These processes typically lead to different final states. For the  $ZZ$ -fusion process, di-Higgs production is detected in association with a muon pair, whereas for the latter fusion process, the double Higgs boson signal is accompanied by missing energy. From kinematic considerations, the  $ZZ$ -fusion contribution is significantly smaller than the  $WW$ -fusion contribution. For these reasons, we focus on the calculation of the partonic process  $W^\pm W^\pm \rightarrow hh$ . The relevant partonic processes are given by

$$\begin{aligned} \hat{\sigma}_{W^\pm W^\mp \rightarrow hh}(s) &= \int d\sigma_{W^\pm W^\mp \rightarrow hh}^T + \int d\sigma_{W^\pm W^\mp \rightarrow hh}^V(\{\alpha, \beta, \dots, \kappa\}, C_{UV}, \lambda) \\ &+ \int d\sigma_{W^\pm W^\mp \rightarrow hh}^T \delta_{\text{soft}}(\lambda \leq E_{\gamma_S} \leq k_c) + \int d\sigma_{W^\pm W^\mp \rightarrow hh}^H(E_{\gamma_S} \geq k_c). \end{aligned} \quad (5)$$

In these formulas,  $d\Phi_2$  denotes the  $2 \rightarrow 2$  phase-space element. In the **GRACE-Loop** program, non-linear gauge-fixing terms have been implemented; see Ref. [62] for more details. As a result, the one-loop amplitude depends on the non-linear gauge parameters and on the ultraviolet-divergent parameter  $C_{UV}$ , whose dependence vanishes when all contributions from the one-loop and counterterm diagrams are taken into account. For the reaction  $W^\pm W^\mp \rightarrow hh$ , virtual photon exchange occurs in the loop, which leads to infrared divergences. The amplitude depends on the photon mass regulator  $\lambda$ . By including soft-photon radiation, the final results become independent of  $\lambda$ . However, the results still depend on the hard-photon cutoff  $k_c$ . To obtain the full one-loop radiative corrections, hard-photon emission must also be taken into account, corresponding to the channel  $W^\pm W^\mp \rightarrow hh\gamma$  with a hard photon in the final state. The final results are free of all the aforementioned parameters. For validation of the calculation, we refer the reader to Appendix A, where explicit results are presented.

Having the corrected partonic cross sections, we evaluate the total cross section by convoluting them with vector W boson PDF as in Eq. 3. We then investigate the effects of the full one-loop electroweak radiative corrections to the processes under consideration. In Fig. 2, the cross sections for the process  $\mu^- \mu^+ \rightarrow W^\pm W^\mp \rightarrow hh$  are shown as a function of the center-of-mass (CoM) energy. In this Figure, the CoM energy is varied from 3 TeV to 30 TeV. The red curve represents the tree-level cross section, while the blue curve shows the fully corrected cross section. We find that the electroweak corrections range from 20% to 30% as the CoM energy increases

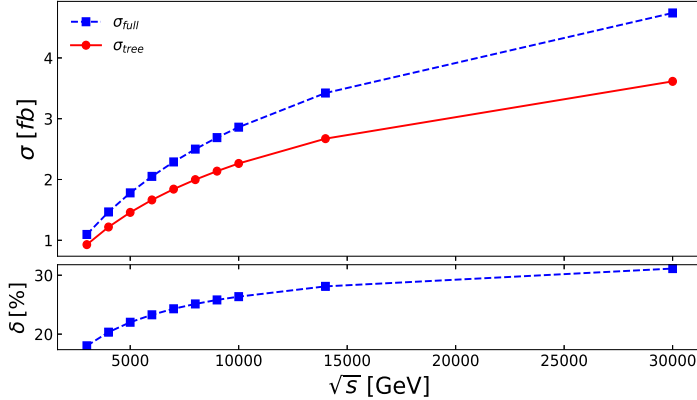


Figure 2: The cross sections for the process  $\mu^- \mu^+ \rightarrow W^\pm W^\mp \rightarrow hh$  and full electroweak radiative corrections are shown as a function of the center-of-mass (CoM) energy.

from 3 TeV to 30 TeV. The differential cross sections with respect to  $p_T^h$  and the rapidity  $\eta^h$  for SM-like Higgs are shown in Figures 3. In these plots, the red line corresponds to the tree-level cross-sections, while the blue line represents the fully corrected cross sections. The left-panel plots show the distributions at  $\sqrt{s} = 3$  TeV, while the right-panel plots present the corresponding ones at  $\sqrt{s} = 10$  TeV. Our finding is that the full electroweak corrections range from  $\sim 10\%$  to  $\sim -30\%$ . In the high- $p_T$  tail region, the cross sections are very small, and the corrections become meaningless in these regions. In principle, the electroweak corrections are of order  $\sim 10\%$  for the distributions mentioned. We find similar corrections for the rapidity distributions.

We have checked that the longitudinal modes  $Z_L Z_L$  and  $W_L^\pm W_L^\pm \rightarrow hh$  provide the dominant contributions in the high-energy regime of future multi-TeV colliders. This conclusion agrees with the numerical results in Ref. [67], in which  $W_L^\pm W_L^\pm \rightarrow hh$  provides a dominant contribution of greater than 97%. For this reason, the  $Q^2$ -dependence of the cross section is rather small, typically at the level of a few percent (same results obtained in Ref. [67]). Last but not least, the cross sections presented in Fig. 2 increase with developing CoM energies due to the Goldstone equivalence theorem.

#### 4. Neutral scalar pair production through vector boson fusion at multi-TeV muon colliders

Neutral scalar pair production through  $W$ -boson fusion at multi-TeV muon colliders within the THDM framework is evaluated in this section. In this work, we limit our calculations to the tree-level cross section for neutral scalar pair production. The amplitudes for the processes are generated by using the `FeynArts/FormCalc` packages [64, 65]. To verify our results, we generate the amplitudes in the general  $R_\xi$  gauge. The results are then tested for gauge invariance by varying the gauge-fixing parameter  $\xi$ . After successfully generating the corresponding amplitudes, we proceed to analyze the phenomenological results in the following subsections.

##### 4.1. $\mu^- \mu^+ \rightarrow W^\pm W^\mp \rightarrow hh$

We first consider SM-like Higgs pair production via  $W$ -boson fusion at multi-TeV muon colliders. For both signal and background processes, the total cross sections for  $\mu^- \mu^+ \rightarrow W^\pm W^\mp \rightarrow hh$  are given by Eq. 3. In the phenomenological analysis, we study the enhancement factor, which is defined as follows:

$$\mu_{hh} = \frac{\sigma_{\mu^- \mu^+ \rightarrow W^\pm W^\mp \rightarrow hh}^{THDM}}{\sigma_{\mu^- \mu^+ \rightarrow W^\pm W^\mp \rightarrow hh}^{SM}} (\mathcal{P}_{THDM}). \quad (6)$$

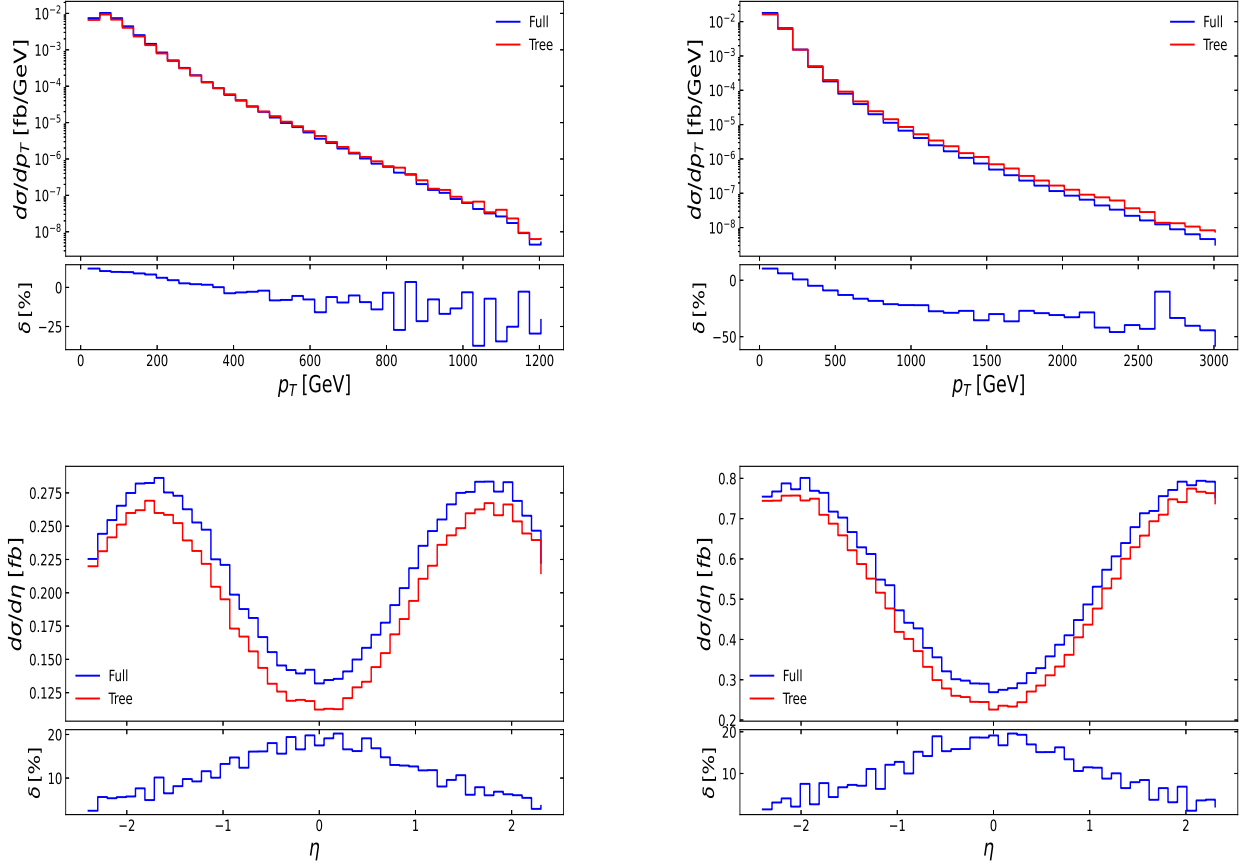


Figure 3: The differential cross sections with respect to  $p_T^h$  and the rapidity  $\eta^h$  are shown. The red line corresponds to the tree-level cross-sections, while the blue line represents the fully corrected cross sections.

Where  $\mathcal{P}_{\text{THDM}} = \{s_{\beta-\alpha}, t_\beta, m_H, m_A, m_{H^\pm}, m_{12}^2\}$ . We are going to study the enhancement factor in the viable parameter space of the THDM obtained in above section. In Fig. 4, the enhancement factor  $\mu^{hh}$  is scanned over  $\tan\beta$  and  $m_H$  for the Type-X THDM shown in the left panels and for the Type-Y THDM shown in the right panels. The results are presented at a center-of-mass energy of 3 TeV in the two upper plots and at 10 TeV in the two lower plots. It is noted that we apply  $p_T^h \geq 20$  GeV and pseudo rapidity  $|\eta_h| < 2.4$ .

The results indicate that the enhancement factor can reach values of up to about 3 for several viable parameter points in the Type-X THDM, whereas it is always smaller than unity in the Type-Y THDM. For the Type-X THDM, we find that the enhancement factor tends to be close to unity when  $\tan\beta \leq 5$  and for  $m_H \geq 400$  GeV, whereas it lies in the range 0.91–0.95 for the Type-Y THDM. In general, this process is the same for the Type-X and Type-Y THDMs, since it does not involve scalar–fermion couplings. The main difference in the observed behavior arises from the distinct allowed parameter spaces, which are primarily constrained by the Yukawa couplings of the scalars to fermions. These results offer interesting prospects for distinguishing between the two types of THDMs through measurements of the production processes at future multi–TeV colliders.

#### 4.2. $\mu^- \mu^+ \rightarrow W^\pm W^\mp \rightarrow AA \rightarrow t\bar{t}b\bar{b}$

In this subsection, we present the computation of the cross sections for  $\mu^- \mu^+ \rightarrow W^\pm W^\mp \rightarrow AA \rightarrow t\bar{t}b\bar{b}$ . As demonstrated in the following paragraphs, we consider the decay channels of the



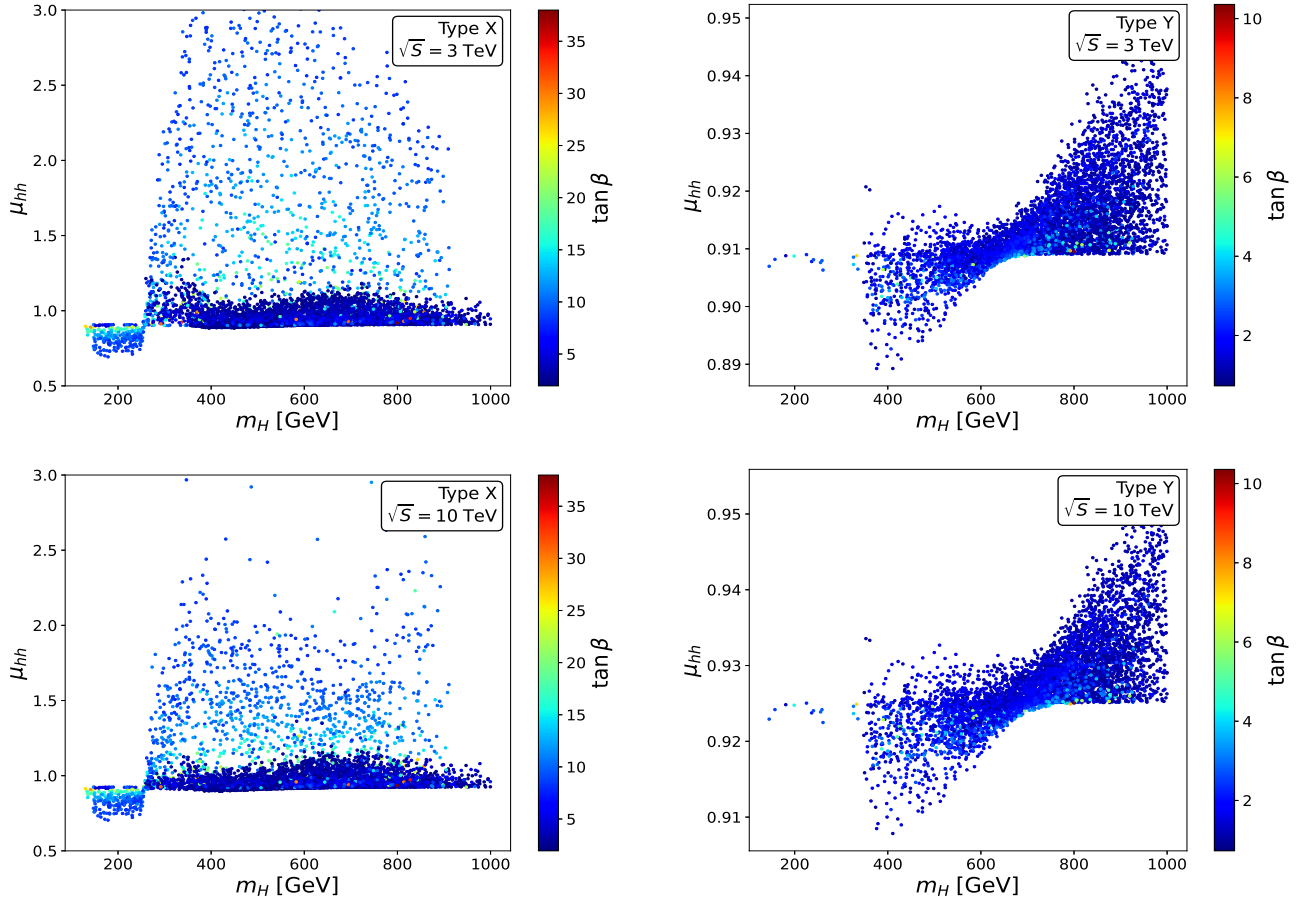


Figure 4: The enhancement factor  $\mu_{hh}$  is scanned over the  $\tan\beta$  and  $m_H$  parameter space, with the Type-X THDM shown in the left panels and the Type-Y THDM shown in the right panels. The results are presented at a center-of-mass energy of 3 TeV in the two upper plots and at 10 TeV in the two lower plots.

CP-odd Higgs,  $A \rightarrow t\bar{t}$  and  $A \rightarrow b\bar{b}$ . The cross section for  $\mu^-\mu^+ \rightarrow W^\pm W^\mp \rightarrow A(p_3)A(p_4) \rightarrow t\bar{t}b\bar{b}$  is evaluated as follows:

$$\begin{aligned}
\sigma_{t\bar{t}b\bar{b}}(s) &= \sum_{\lambda_1, \lambda_2} \int_{\frac{4m_A^2}{s}}^1 d\tau \int_{\tau}^1 \frac{d\xi}{\xi} f_{W_{\lambda_1}/\mu}(\xi, Q^2) f_{W_{\lambda_2}/\mu}\left(\frac{\tau}{\xi}, Q^2\right) \times \\
&\times (2!) \int_{4m_t^2}^{\hat{s}} \frac{dp_3^2}{\pi} \frac{m_A \Gamma_{A \rightarrow t\bar{t}}}{(p_3^2 - m_A^2)^2 + \Gamma_A^2 m_A^2} \times \\
&\times \int_{4m_b^2}^{(\sqrt{\hat{s}} - \sqrt{p_3^2})^2} \frac{dp_4^2}{\pi} \frac{m_A \Gamma_{A \rightarrow b\bar{b}}}{(p_4^2 - m_A^2)^2 + \Gamma_A^2 m_A^2} \times \\
&\times \frac{1}{2!} \int d\Phi_3 \left| \mathcal{M}_{W_{\lambda_1} W_{\lambda_2} \rightarrow A(p_3)A(p_4) \rightarrow t\bar{t}b\bar{b}}(\hat{s} = \tau s) \right|^2. \tag{7}
\end{aligned}$$

Here,  $\Gamma_{A \rightarrow b\bar{b}}$ ,  $\Gamma_{A \rightarrow t\bar{t}}$ , and  $\Gamma_A$  denote the partial decay widths of the CP-odd Higgs boson into  $b\bar{b}$  and  $t\bar{t}$ , and its total decay width, respectively. All the decay widths mentioned above are calculated using the public code H-COUP [63]. Note that a factor of 2 is included to account for

the interchange of the decay modes  $A \rightarrow b\bar{b}$  and  $A \rightarrow t\bar{t}$ , while an additional factor of 1/2 arises from the presence of two identical CP-odd Higgs bosons in the final state of the partonic process  $W^\pm W^\mp \rightarrow AA$ . We also emphasize that off-shell CP-odd Higgs bosons (i.e.,  $p_3^2 \neq m_A^2$  and  $p_4^2 \neq m_A^2$ ) are taken into account in this procedure. The partonic process is first generated in the general  $\mathcal{R}_\xi$  gauge with the help of the computer algebra packages `FeynArts/FormCalc` [64, 65]. The results are then checked for consistency by varying the  $\xi$ -gauge parameters. The corrected amplitude for the process under consideration is convoluted as in Eq. 7.

The branching ratios for the decays  $A \rightarrow t\bar{t}$  (left panel) and  $A \rightarrow b\bar{b}$  (right panel) are shown in the parameter space of  $m_A$  and  $\tan\beta$ . The results for the Type-X THDM are presented in the upper panels, while the corresponding decay rates for the Type-Y THDM are shown in the lower panels. In all cases, the decay  $A \rightarrow t\bar{t}$  is dominant compared to  $A \rightarrow b\bar{b}$ . We also find that the branching ratios for  $A \rightarrow b\bar{b}$  in the Type-Y THDM are larger by more than two orders of magnitude than those in the Type-X THDM. This behavior can be understood from the different Yukawa coupling structures in the two models.

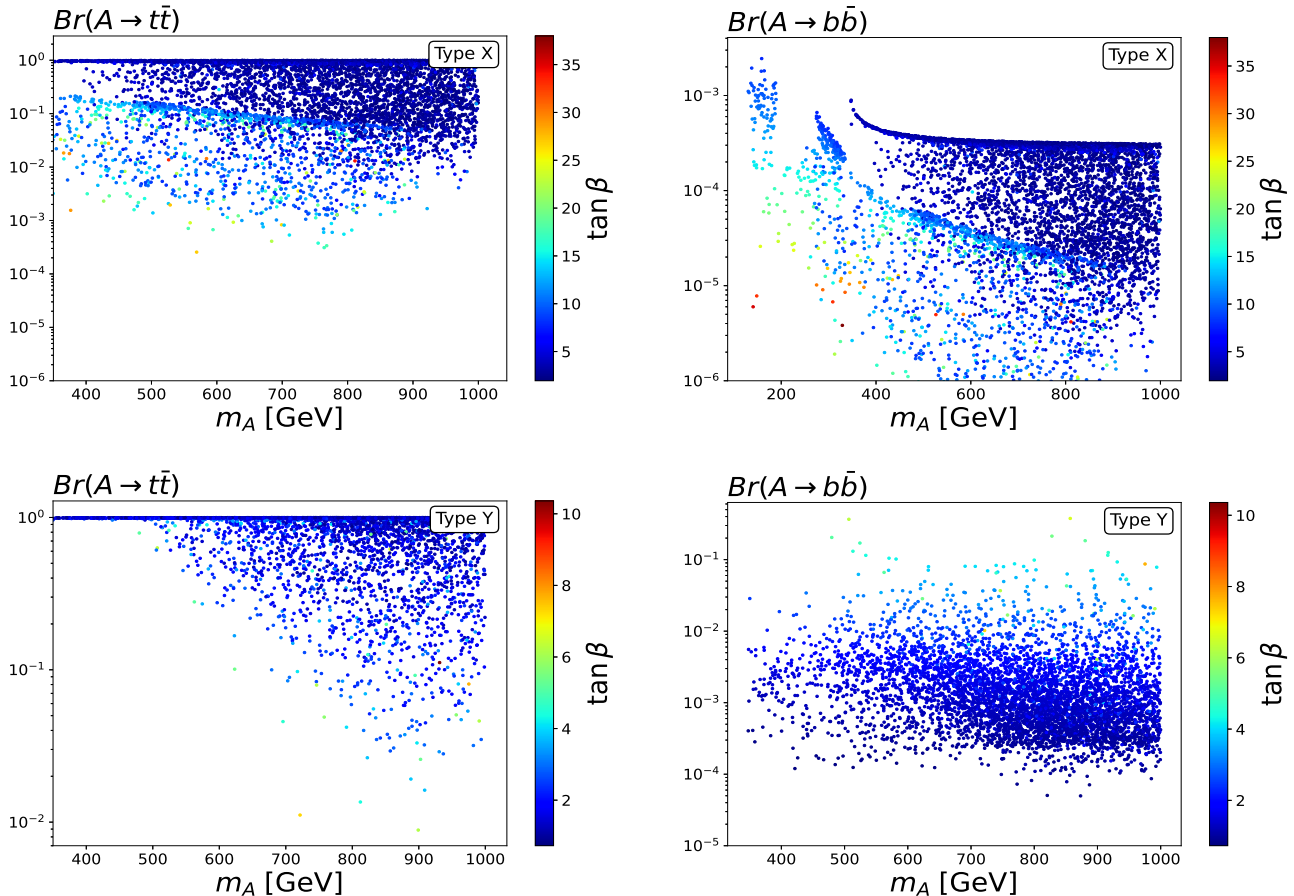


Figure 5: The branching ratios for the decays  $A \rightarrow t\bar{t}$  (left panel) and  $A \rightarrow b\bar{b}$  (right panel) are shown in the parameter space of  $m_A$  and  $\tan\beta$ . The results for the Type-X THDM are presented in the upper panels, while the corresponding decay rates for the Type-Y THDM are shown in the lower panels.

We turn our attention to the generation of events for  $\mu^-\mu^+ \rightarrow W^\pm W^\mp \rightarrow A(p_3)A(p_4) \rightarrow t\bar{t}b\bar{b}$ , which are scanned over the parameter space of the Type-X and Type-Y THDMs. In Fig. 6, we present the event distributions at  $\sqrt{s} = 3$  TeV with an integrated luminosity of  $\mathcal{L} = 3000 \text{ fb}^{-1}$  and at  $\sqrt{s} = 10$  TeV with  $\mathcal{L} = 10000 \text{ fb}^{-1}$ . The results for the Type-X THDM are shown in the upper

two panels, while those for the Type-Y THDM are displayed in the lower two panels. The events are plotted in the parameter space of CP-odd Higgs mass  $m_A$  and the mixing angle  $\tan \beta$ . In these plots, the SM background events are shown as red dotted lines. For the SM background cross-sections, we consider the corresponding processes  $\mu^- \mu^+ \rightarrow W^\pm W^\mp \rightarrow t\bar{t}b\bar{b}$ . The SM background cross sections are evaluated after applying the appropriate kinematic cuts, as described below. To identify the top- and bottom-quark pairs originating from the CP-odd Higgs boson, we apply invariant-mass cuts on the final-state particles,  $|m_{t\bar{t}} - m_A| \leq 20$  GeV,  $|m_{b\bar{b}} - m_A| \leq 20$  GeV. These cuts effectively reduce the SM background, since the SM cross sections are calculated far from the dominant resonance peaks associated with  $Z$ -boson mediating. Furthermore, the kinematic cuts are applied the transverse momentum  $p_T^{b/\bar{b}} \geq 20$  GeV, the rapidity  $|\eta^{b/\bar{b}}| \leq 2.4$  for bottom-quarks ( $\bar{b}$ -quarks).

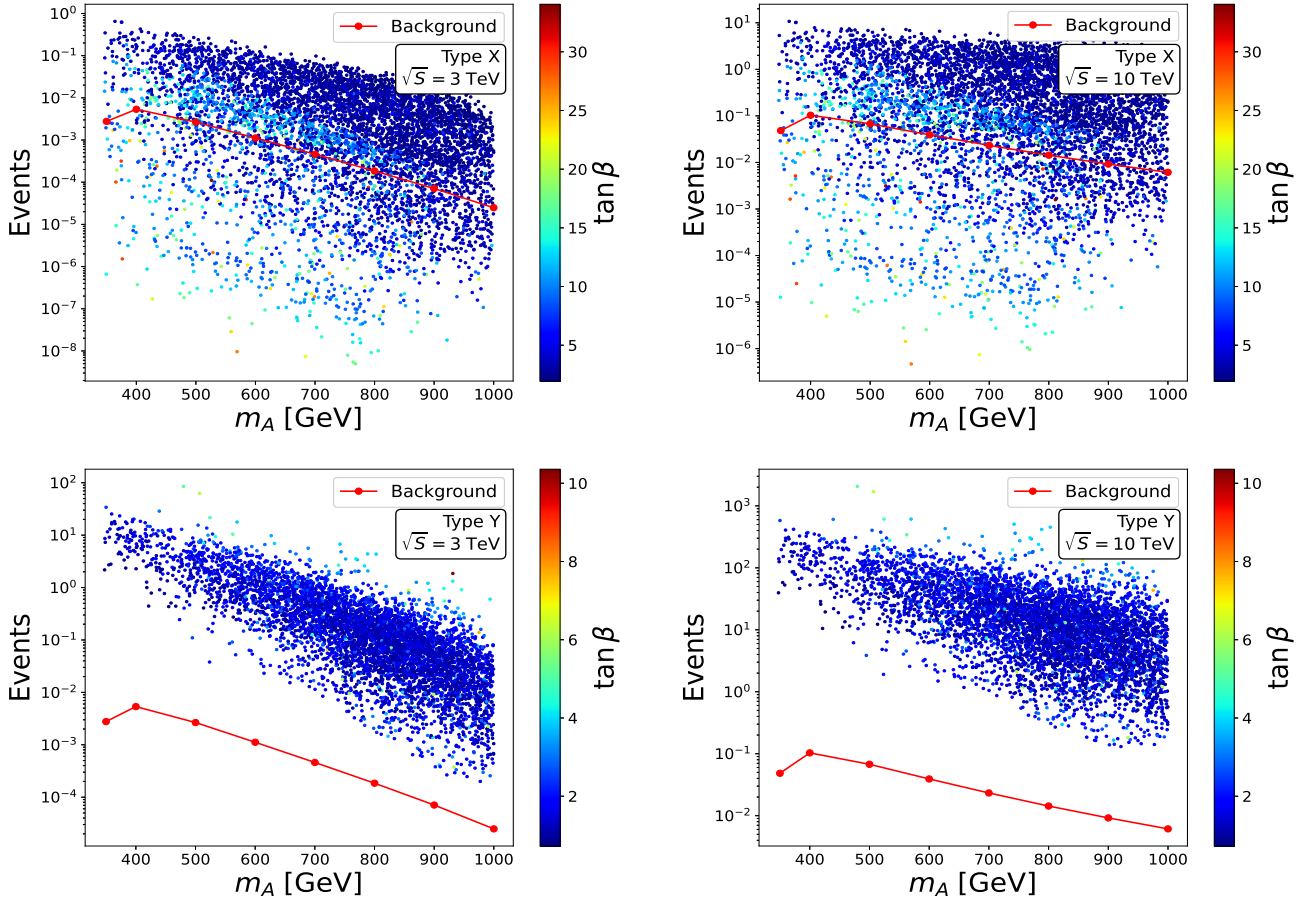


Figure 6: The event distributions at  $\sqrt{s} = 3$  TeV with an integrated luminosity of  $\mathcal{L} = 3000 \text{ fb}^{-1}$  and at  $\sqrt{s} = 10$  TeV with  $\mathcal{L} = 10000 \text{ fb}^{-1}$ . The results for the Type-X THDM are shown in the upper two panels, while those for the Type-Y THDM are displayed in the lower two panels.

In all cases, the pair production of CP-odd Higgs bosons in the Type-Y THDM at  $\sqrt{s} = 10$  TeV multi-TeV muon collider is a promising channel that can be tested at future colliders. In this case, we observe that the Standard Model background is rather small and it can therefore be neglected. Moreover, we consider the top-quark decay into a charged lepton, its associated neutrino, and a bottom quark, for which the total branching fraction is 0.332 (taken from [66]). The final state is  $\ell\bar{\ell}b\bar{b}b\bar{b}$  accompanied by missing energy. The statistical significance for the process  $\mu^- \mu^+ \rightarrow W^\pm W^\mp \rightarrow AA \rightarrow t\bar{t}b\bar{b} \rightarrow \ell\bar{\ell}b\bar{b}b\bar{b}$  including missing energy is estimated as

$\mathcal{S} = \sqrt{\mathcal{L} \cdot \sigma \times [\text{Br}(t \rightarrow \ell \nu_\ell b)]^2}$ . In Fig. 7, the significances are scanned over the valid parameter space in correlation with the enhancement factor  $\mu_{hh}$ . We find that the signal can be observed with a significance exceeding  $2\sigma$  at several parameter points within the viable parameter space of the Type-Y THDM. However, almost all viable parameter points lie below the  $5\sigma$  significance level.

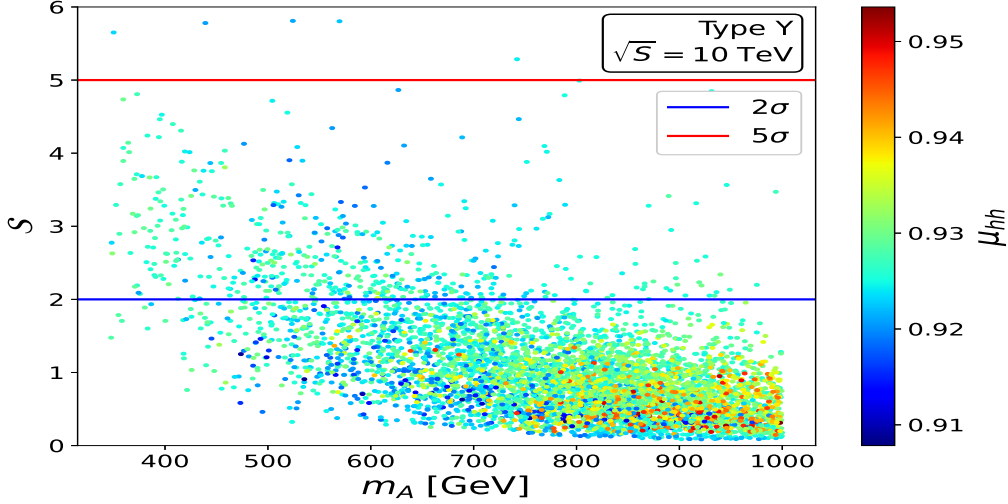


Figure 7: The statistical significances of the signal process  $\mu^- \mu^+ \rightarrow W^\pm W^\mp \rightarrow AA \rightarrow t\bar{t}b\bar{b} \rightarrow \ell\bar{\ell}b\bar{b}b\bar{b}$  including missing energy are scanned over the valid parameter space in correlation with the enhancement factor  $\mu_{hh}$  for the Type-Y THDM at  $\sqrt{s} = 10$  TeV.

## 5. Conclusions

We present the first results for full one-loop electroweak radiative corrections to  $\mu^- \mu^+ \rightarrow W^\pm W^\mp \rightarrow hh$  in the Standard Model in this work. We then evaluate neutral scalar pair production through vector boson fusion at multi-TeV muon colliders in the THDM. In the phenomenological analysis, the enhancement factors for SM-like Higgs pair production in the THDM with respect to the corresponding ones in the SM are scanned over the parameter space within the viable regions of the Type-X and Type-Y THDMs. Our findings show that the ratio can reach a factor of 3 in several regions within the valid parameter space of the Type-X THDM, whereas it lies in the range 0.91 to 0.96 over the entire parameter space of the Type-Y THDM. Finally, we evaluate CP-odd Higgs pair production through vector  $W$ -boson fusion at multi-TeV muon colliders. In the Type-Y case at  $\sqrt{s} = 10$  TeV with an integrated luminosity of  $\mathcal{L} = 10000 \text{ fb}^{-1}$ , CP-odd Higgs pair production in the  $t\bar{t}b\bar{b}$  final state, with subsequent top-quark decays into leptons and bottom quarks taken into account, can be tested with a statistical significance exceeding the  $2\sigma$  level at several viable parameter points. This provides a promising possibility to probe the scalar Higgs sector and deepen our understanding of electroweak symmetry-breaking dynamics in particle physics.

**Acknowledgment:** This research is funded by Vietnam National Foundation for Science and Technology Development (NAFOSTED) under the grant number 103.01-2023.16.

## Appendix A: Numerical Consistency Checks

In this paper, we use the input parameters from Particle Data Group [66]. We are working in  $G_\mu$ -scheme where the Fine-Structure Constant is calculated as

$$\alpha = \sqrt{2}G_F m_W^2 \left(1 - \frac{m_W^2}{m_Z^2}\right) / \pi \quad (8)$$

with  $G_F = 1.1663785 \cdot 10^{-5} \text{ GeV}^{-2}$ .

In this Appendix, we present numerical consistency checks for the one-loop radiative corrections to the process  $\mu^- \mu^+ \rightarrow W^\pm W^\mp \rightarrow hh$  in the SM. The **GRACE-Loop** system implements non-linear gauge (NLG) fixing terms in the Lagrangian. As a result, the total cross section must be independent of the NLG parameters, namely  $\alpha, \beta, \dots$ , and  $\kappa$ . In the context of one-loop renormalization, the total cross section is also free of ultraviolet (UV) divergences ( $C_{UV}$ ). Due to the presence of virtual photon exchange in the loop, the corresponding Feynman diagrams contain infrared divergences. By including soft-photon radiation, the cross sections become independent of  $\lambda$  (the photon mass). However, the inclusion of soft-photon radiation makes the cross section dependent on the photon energy cutoff parameter, denoted by  $k_c$ . At this stage, the dependence on  $k_c$  is canceled by the contribution from hard-photon radiation. In the final result, the fully corrected cross sections are free of all the above-mentioned parameters.

In Table 1, we present numerical checks of the NLG parameters  $\alpha, \beta, \dots$ , and  $\kappa$ , as well as  $C_{UV}$  and  $\lambda$ . The results show that the cross sections exhibit good stability when these parameters are varied over wide ranges. It is noted that we apply  $p_T^h \geq 20 \text{ GeV}$  and pseudorapidity  $|\eta_h| < 2.4$ . The tests are performed at a center-of-mass energy of 3 TeV at a future multi-TeV muon collider.

$(\{\alpha, \beta, \dots, \kappa\}, C_{UV}, \lambda)$	$\sigma_{\mu^- \mu^+ \rightarrow W^\pm W^\mp \rightarrow hh}^V$	$\sigma_{\mu^- \mu^+ \rightarrow W^\pm W^\mp \rightarrow hh}^S$	$\sigma_{\mu^- \mu^+ \rightarrow W^\pm W^\mp \rightarrow hh}^{V+S}$
$(\{0, 0, 0, 0, 0\}, 0, 10^{-13})$	$-2.97(2) \cdot 10^{-4}$	$2.61(7) \cdot 10^{-4}$	$-0.35(6) \cdot 10^{-4}$
$(\{1, 2, 3, 4, 5\}, 10^2, 10^{-15})$	$-3.50(5) \cdot 10^{-4}$	$3.15(0) \cdot 10^{-4}$	$-0.35(5) \cdot 10^{-4}$
$(\{10, 20, 30, 40, 50\}, 10^3, 10^{-17})$	$-4.04(0) \cdot 10^{-4}$	$3.68(4) \cdot 10^{-4}$	$-0.35(6) \cdot 10^{-4}$

Table 1: Numerical consistency checks for the one-loop radiative corrections to the process  $\mu^- \mu^+ \rightarrow W^\pm W^\mp \rightarrow hh$  in the SM are presented. In this table, we vary  $(\alpha, \beta, \dots, \kappa)$ ,  $C_{UV}$ , and  $\lambda$  in the first column. The second (third) column corresponds to the virtual one-loop corrections (soft-photon radiation) in pb, while the last column shows the sum of these contributions in pb. We note that  $\sigma_{\mu^- \mu^+ \rightarrow W^\pm W^\mp \rightarrow hh}^T = 9.64(3) \times 10^{-4} \text{ pb}$ .

In Table 2, tests of the  $k_c$  stability of the results are shown. In the first column, we vary  $k_c$  from  $10^{-3} \text{ GeV}$  to  $10^{-5} \text{ GeV}$ . The soft-photon contributions are presented in the second column, while the hard-photon contributions are shown in the third column. The last column shows the sum of these cross sections. All cross sections are given in pb. We fix  $(0, 0, 0, 0, 0, 0, 10^{-15})$  for this test. We find that the results exhibit good stability under variations of the photon energy cutoff parameter.

$k_c$ [GeV]	$\sigma_{\mu^+\mu^-\rightarrow W^\pm W^\mp\rightarrow hh}^S$	$\sigma_{\mu^+\mu^-\rightarrow W^\pm W^\mp\rightarrow hh}^H$	$\sigma_{\mu^+\mu^-\rightarrow W^\pm W^\mp\rightarrow hh}^{S+H}$
$10^{-3}$	$3.15(0) \cdot 10^{-4}$	$1.315(2) \cdot 10^{-4}$	$4.46(5) \cdot 10^{-4}$
$10^{-4}$	$2.88(3) \cdot 10^{-4}$	$1.581(8) \cdot 10^{-4}$	$4.46(5) \cdot 10^{-4}$
$10^{-5}$	$2.61(7) \cdot 10^{-4}$	$1.84(8) \cdot 10^{-4}$	$4.46(5) \cdot 10^{-4}$

Table 2: Test of the  $k_c$  stability of the results. In the first column, we change  $k_c$  from  $10^{-3}$  GeV to  $10^{-5}$  GeV. The soft-photon results are presented in the second column, while the hard contributions are shown in the third column. The last column shows the sum of these cross sections. All cross sections are shown in pb. We fix  $(0, 0, 0, 0, 0, 0, 10^{-15})$  for the test.

## Appendix B: Comparison with previous references

The tree-level process  $\mu^-\mu^+ \rightarrow W^\pm W^\mp \rightarrow hh$  in the SM has been studied in many earlier works. We cross-check the tree-level cross section computed in this work with the results reported in Ref. [67]. In Table 3, the first column shows the center-of-mass energies ranging from 4 TeV to 30 TeV. The second column presents our results obtained in this work, while the third column lists the results from Ref. [67]. The data indicates that our results are in good agreement with those of Ref. [67]. The last column shows the difference between the two results, expressed in percent. We find that the difference between the two results is only a few percent. This is due to the scale dependence of the results, which is also at the level of a few percent, as pointed out in Ref. [67]. No cuts are applied to the final-state Higgs bosons for the results shown in the first row, whereas the results in the second row include the additional requirement that the invariant mass of the two final-state Higgs bosons be greater than 1 TeV.

$\sqrt{s}$ [TeV]	This work	Ref. [67]	$\delta$ [%]
4	$1.9374 \pm 0.0008$	2.03	4.6%
	$0.341 \pm 0.002$	0.364	6.3%
14	$5.830 \pm 0.003$	6.01	3.0%
	$2.391 \pm 0.001$	2.44	2.0%
30	$9.390 \pm 0.006$	9.48	0.95%
	$4.784 \pm 0.003$	4.63	3.1%

Table 3: Tree-level process  $\mu^-\mu^+ \rightarrow W^\pm W^\mp \rightarrow hh$  in this work and in Ref. [67]. The cross sections are shown in fb. The results in the second row are the same as those in the first row, but with the additional requirement that the invariant mass of the two final-state Higgs bosons be greater than 1 TeV.

## References

- [1] G. Aad *et al.* [ATLAS], Phys. Rev. D **106** (2022) no.5, 052001 doi:10.1103/PhysRevD.106.052001 [arXiv:2112.11876 [hep-ex]].
- [2] G. Aad *et al.* [ATLAS], JHEP **01** (2024), 066 doi:10.1007/JHEP01(2024)066 [arXiv:2310.12301 [hep-ex]].
- [3] G. Aad *et al.* [ATLAS], Eur. Phys. J. C **83** (2023) no.6, 519 doi:10.1140/epjc/s10052-023-11559-y [arXiv:2210.05415 [hep-ex]].

- [4] A. Tumasyan *et al.* [CMS], Phys. Rev. Lett. **131** (2023) no.4, 041803 doi:10.1103/PhysRevLett.131.041803 [arXiv:2205.06667 [hep-ex]].
- [5] A. Tumasyan *et al.* [CMS], Phys. Rev. Lett. **129** (2022) no.8, 081802 doi:10.1103/PhysRevLett.129.081802 [arXiv:2202.09617 [hep-ex]].
- [6] G. Aad *et al.* [ATLAS], JHEP **07** (2023), 040 doi:10.1007/JHEP07(2023)040 [arXiv:2209.10910 [hep-ex]].
- [7] G. Aad *et al.* [ATLAS], Phys. Rev. D **108** (2023) no.5, 052003 doi:10.1103/PhysRevD.108.052003 [arXiv:2301.03212 [hep-ex]].
- [8] G. Aad *et al.* [ATLAS], Phys. Rev. Lett. **132** (2024) no.23, 231801 doi:10.1103/PhysRevLett.132.231801 [arXiv:2311.15956 [hep-ex]].
- [9] G. Aad *et al.* [ATLAS], JHEP **02** (2024), 037 doi:10.1007/JHEP02(2024)037 [arXiv:2310.11286 [hep-ex]].
- [10] G. Aad *et al.* [ATLAS], Phys. Lett. B **858** (2024), 139007 doi:10.1016/j.physletb.2024.139007 [arXiv:2404.17193 [hep-ex]].
- [11] G. Aad *et al.* [ATLAS], JHEP **08** (2024), 164 doi:10.1007/JHEP08(2024)164 [arXiv:2405.20040 [hep-ex]].
- [12] G. Aad *et al.* [ATLAS], Phys. Rev. D **110** (2024) no.3, 032012 doi:10.1103/PhysRevD.110.032012 [arXiv:2404.12660 [hep-ex]].
- [13] A. Hayrapetyan *et al.* [CMS], JHEP **10** (2024), 061 doi:10.1007/JHEP10(2024)061 [arXiv:2404.08462 [hep-ex]].
- [14] G. Aad *et al.* [ATLAS], [arXiv:2507.03495 [hep-ex]].
- [15] A. Tumasyan *et al.* [CMS], JHEP **02** (2025), 040 doi:10.1007/JHEP02(2025)040 [arXiv:2407.13872 [hep-ex]].
- [16] S. Iguro, T. Kitahara, Y. Omura and H. Zhang, Phys. Rev. D **107** (2023) no.7, 075017 doi:10.1103/PhysRevD.107.075017 [arXiv:2211.00011 [hep-ph]].
- [17] B. Guo, X. Sun, L. Zhang, Z. Li and Y. Ban, Phys. Rev. D **107** (2023) no.3, 034014 doi:10.1103/PhysRevD.107.034014 [arXiv:2207.10912 [hep-ph]].
- [18] R. Gómez-Ambrosio, F. J. Llanes-Estrada, A. Salas-Bernárdez and J. J. Sanz-Cillero, Phys. Rev. D **106** (2022) no.5, 053004 doi:10.1103/PhysRevD.106.053004 [arXiv:2204.01763 [hep-ph]].
- [19] L. Huang, S. b. Kang, J. H. Kim, K. Kong and J. S. Pi, JHEP **08** (2022), 114 doi:10.1007/JHEP08(2022)114 [arXiv:2203.11951 [hep-ph]].
- [20] D. Domenech, M. J. Herrero, R. A. Morales and M. Ramos, Phys. Rev. D **106** (2022) no.11, 115027 doi:10.1103/PhysRevD.106.115027 [arXiv:2208.05452 [hep-ph]].
- [21] R. Gómez-Ambrosio, F. J. Llanes-Estrada, A. Salas-Bernárdez and J. J. Sanz-Cillero, Commun. Theor. Phys. **75** (2023) no.9, 095202 doi:10.1088/1572-9494/ace95e [arXiv:2207.09848 [hep-ph]].

- [22] L. Alasfar, L. Cadamuro, C. Dimitriadi, A. Ferrari, R. Gröber, G. Heinrich, T. I. Carlson, J. Lang, S. Ördek and L. P. Sánchez, *et al.* SciPost Phys. Comm. Rep. **2024** (2024), 2 doi:10.21468/SciPostPhysCommRep.2 [arXiv:2304.01968 [hep-ph]].
- [23] H. Abouabid, A. Arhrib, D. Azevedo, J. E. Falaki, P. M. Ferreira, M. Mühlleitner and R. Santos, JHEP **09** (2022), 011 doi:10.1007/JHEP09(2022)011 [arXiv:2112.12515 [hep-ph]].
- [24] F. Feuerstake, E. Fuchs, T. Robens and D. Winterbottom, JHEP **04** (2025), 094 doi:10.1007/JHEP04(2025)094 [arXiv:2409.06651 [hep-ph]].
- [25] A. Arhrib, A. Hmissou, S. Moretti and L. Rahili, [arXiv:2511.03902 [hep-ph]].
- [26] A. Dedes, J. Rosiek and M. Ryzkowski, Phys. Rev. D **112** (2025) no.5, 055044 doi:10.1103/bywd-2dy1 [arXiv:2506.12917 [hep-ph]].
- [27] J. Kriewald, E. Pinsard and A. M. Teixeira, [arXiv:2512.16734 [hep-ph]].
- [28] F. Esser, M. Madigan, A. Salas-Bernardez, V. Sanz and M. Ubiali, JHEP **10** (2024), 164 doi:10.1007/JHEP10(2024)164 [arXiv:2404.08062 [hep-ph]].
- [29] M. Belfkir, [arXiv:2512.17874 [hep-ph]].
- [30] H. T. Li, Z. G. Si, J. Wang, X. Zhang and D. Zhao, Phys. Lett. B **868** (2025), 139776 doi:10.1016/j.physletb.2025.139776 [arXiv:2503.22001 [hep-ph]].
- [31] Z. Hu and T. Liu, [arXiv:2509.06381 [hep-ph]].
- [32] M. Bonetti, G. Heinrich, S. Jones, M. Kerner, P. Rendler, T. Stone and A. Vestner, [arXiv:2511.15267 [hep-ph]].
- [33] J. Braun, P. Brecht, G. Heinrich, M. Höfer, B. Jäger, A. Karlberg and S. Reinhardt, [arXiv:2511.02488 [hep-ph]].
- [34] I. Brivio, R. Gröber and K. Schmid, [arXiv:2511.23411 [hep-ph]].
- [35] J. Braun, P. Brecht, G. Heinrich and M. Höfer, JHEP **07** (2025), 209 doi:10.1007/JHEP07(2025)209 [arXiv:2502.09132 [hep-ph]].
- [36] A. Bhattacharya, F. Campanario, S. Carlotti, J. Chang, J. Mazzitelli, M. Mühlleitner, J. Ronca and M. Spira, [arXiv:2512.14823 [hep-ph]].
- [37] R. Bonciani, G. Degrassi, P. P. Giardino and R. Gröber, Phys. Rev. Lett. **121** (2018) no.16, 162003 doi:10.1103/PhysRevLett.121.162003 [arXiv:1806.11564 [hep-ph]].
- [38] J. Davies, K. Schönwald and M. Steinhauser, JHEP **08** (2025), 192 doi:10.1007/JHEP08(2025)192 [arXiv:2503.17449 [hep-ph]].
- [39] Z. Hu, T. Liu and J. M. Yang, JHEP **09** (2025), 132 doi:10.1007/JHEP09(2025)132 [arXiv:2503.10051 [hep-ph]].
- [40] S. Jaskiewicz, S. Jones, R. Szafron and Y. Ulrich, JHEP **09** (2025), 015 doi:10.1007/JHEP09(2025)015 [arXiv:2501.00587 [hep-ph]].



- [41] J. Davies, K. Schönwald, M. Steinhauser and M. Vitti, *JHEP* **08** (2024), 096 doi:10.1007/JHEP08(2024)096 [arXiv:2405.20372 [hep-ph]].
- [42] E. Bagnaschi, G. Degrossi and R. Gröber, *Eur. Phys. J. C* **83** (2023) no.11, 1054 doi:10.1140/epjc/s10052-023-12238-8 [arXiv:2309.10525 [hep-ph]].
- [43] J. Davies, F. Herren, G. Mishima and M. Steinhauser, *JHEP* **01** (2022), 049 doi:10.1007/JHEP01(2022)049 [arXiv:2110.03697 [hep-ph]].
- [44] B. Das, S. Moretti, S. Munir and P. Poulose, *Eur. Phys. J. C* **81** (2021) no.4, 347 doi:10.1140/epjc/s10052-021-09023-w [arXiv:2012.09587 [hep-ph]].
- [45] G. Wang, Y. Wang, X. Xu, Y. Xu and L. L. Yang, *Phys. Rev. D* **104** (2021) no.5, L051901 doi:10.1103/PhysRevD.104.L051901 [arXiv:2010.15649 [hep-ph]].
- [46] J. Baglio, F. Campanario, S. Glaus, M. Mühlleitner, J. Ronca and M. Spira, *Phys. Rev. D* **103** (2021) no.5, 056002 doi:10.1103/PhysRevD.103.056002 [arXiv:2008.11626 [hep-ph]].
- [47] J. Baglio, F. Campanario, S. Glaus, M. Mühlleitner, J. Ronca, M. Spira and J. Streicher, *JHEP* **04** (2020), 181 doi:10.1007/JHEP04(2020)181 [arXiv:2003.03227 [hep-ph]].
- [48] L. B. Chen, H. T. Li, H. S. Shao and J. Wang, *JHEP* **03** (2020), 072 doi:10.1007/JHEP03(2020)072 [arXiv:1912.13001 [hep-ph]].
- [49] P. Basler, S. Dawson, C. Englert and M. Mühlleitner, *Phys. Rev. D* **101** (2020) no.1, 015019 doi:10.1103/PhysRevD.101.015019 [arXiv:1909.09987 [hep-ph]].
- [50] L. B. Chen, H. T. Li, H. S. Shao and J. Wang, *Phys. Lett. B* **803** (2020), 135292 doi:10.1016/j.physletb.2020.135292 [arXiv:1909.06808 [hep-ph]].
- [51] D. T. Tran, Q. H. M. Pham, K. N. T. Ho and K. H. Phan, [arXiv:2509.08417 [hep-ph]].
- [52] D. T. Tran, Q. H. M. Pham, K. N. T. Ho and K. H. Phan, [arXiv:2509.23877 [hep-ph]].
- [53] K. H. Phan and Q. H. M. Pham, [arXiv:2511.14525 [hep-ph]].
- [54] Q. H. M. Pham, K. N. T. Ho and K. H. Phan, [arXiv:2512.03810 [hep-ph]].
- [55] G. C. Branco, P. M. Ferreira, L. Lavoura, M. N. Rebelo, M. Sher and J. P. Silva, *Phys. Rept.* **516** (2012), 1-102 doi:10.1016/j.physrep.2012.02.002 [arXiv:1106.0034 [hep-ph]].
- [56] M. Aoki, S. Kanemura, K. Tsumura and K. Yagyu, *Phys. Rev. D* **80** (2009), 015017 doi:10.1103/PhysRevD.80.015017 [arXiv:0902.4665 [hep-ph]].
- [57] M. E. Peskin and T. Takeuchi, *Phys. Rev. D* **46** (1992), 381-409 doi:10.1103/PhysRevD.46.381
- [58] D. Eriksson, J. Rathsman and O. Stal, *Comput. Phys. Commun.* **181** (2010), 189-205 doi:10.1016/j.cpc.2009.09.011 [arXiv:0902.0851 [hep-ph]].
- [59] P. Bechtle, D. Dercks, S. Heinemeyer, T. Klingl, T. Stefaniak, G. Weiglein and J. Wittbrodt, *Eur. Phys. J. C* **80** (2020) no.12, 1211 doi:10.1140/epjc/s10052-020-08557-9 [arXiv:2006.06007 [hep-ph]].

- [60] P. Bechtle, S. Heinemeyer, T. Klingl, T. Stefaniak, G. Weiglein and J. Wittbrodt, Eur. Phys. J. C **81** (2021) no.2, 145 doi:10.1140/epjc/s10052-021-08942-y [arXiv:2012.09197 [hep-ph]].
- [61] F. Mahmoudi, Comput. Phys. Commun. **180** (2009), 1579-1613 doi:10.1016/j.cpc.2009.02.017 [arXiv:0808.3144 [hep-ph]].
- [62] G. Belanger, F. Boudjema, J. Fujimoto, T. Ishikawa, T. Kaneko, K. Kato and Y. Shimizu, Phys. Rept. **430** (2006), 117-209 doi:10.1016/j.physrep.2006.02.001 [arXiv:hep-ph/0308080 [hep-ph]].
- [63] M. Aiko, S. Kanemura, M. Kikuchi, K. Sakurai and K. Yagyu, Comput. Phys. Commun. **301** (2024), 109231 doi:10.1016/j.cpc.2024.109231 [arXiv:2311.15892 [hep-ph]].
- [64] T. Hahn, Comput. Phys. Commun. **140** (2001), 418-431 doi:10.1016/S0010-4655(01)00290-9 [arXiv:hep-ph/0012260 [hep-ph]].
- [65] T. Hahn and M. Perez-Victoria, Comput. Phys. Commun. **118** (1999), 153-165 doi:10.1016/S0010-4655(98)00173-8 [arXiv:hep-ph/9807565 [hep-ph]].
- [66] S. Navas *et al.* [Particle Data Group], Phys. Rev. D **110** (2024) no.3, 030001 doi:10.1103/PhysRevD.110.030001
- [67] R. Ruiz, A. Costantini, F. Maltoni and O. Mattelaer, JHEP **06** (2022), 114 doi:10.1007/JHEP06(2022)114 [arXiv:2111.02442 [hep-ph]].